Properties of a multiterminal superconducting nanostructure with a double quantum dot

G. Górski, K. Kucab, and T. Domański, and T. Domański

¹Institute of Physics, Faculty of Exact and Technical Sciences, University of Rzeszów, 35-310 Rzeszów, Poland ²Institute of Physics, M. Curie-Skłodowska University, 20-031 Lublin, Poland

(Received 16 April 2025; accepted 5 November 2025; published 1 December 2025)

We study the charge transport and thermoelectric properties of a junction comprising a double quantum dot embedded in T-shaped geometry on the interface between two normal/ferromagnetic electrodes and a superconducting lead. We show that the interdot coupling plays a major role in controlling the local and nonlocal transport properties of this setup. For the weak interdot coupling limit, we obtain the interferometric (Fano-type) line shapes imprinted in the quasiparticle spectra, conductances, and Seebeck coefficients. In contrast, for strong interdot coupling, we predict that the local and nonlocal transport coefficients are primarily dependent on the molecular Andreev bound states induced by the superconducting proximity effect simultaneously in both quantum dots.

DOI: 10.1103/lc6p-2f7g

I. INTRODUCTION

Charge transport through superconducting heterostructures comprising quantum dots (QDs) is currently being intensively explored due to possible applications in nanoelectronics, spintronics, metrology, and quantum information processing [1]. Various configurations of QDs coupled to either conventional [2,3] or topological superconductors [4,5] are being considered, offering the realization of brand-new technological devices.

The transport properties of hybrid structures where QDs are between superconducting (S) and normal (N) or ferromagnetic (F) electrodes are essentially affected by the bound states [6,7], enabling subgap charge transfer via electron-tohole (Andreev) scattering [8–11]. Such in-gap states originate from the superconducting proximity effect. Competition with the on-dot Coulomb repulsion, however, can lead, under specific conditions, to the single occupancy of a QD, allowing for the Kondo state to emerge [6,12,13]. Signatures of these Andreev and Kondo effects have been observed in various nanostructures [14–16]. With the variation of the energy level or hybridization to external leads the ground state of a QD can change from the single occupied configuration to the BCS-type configuration that is manifested by a crossing of the in-gap states [6]. At such a parity crossing the lowtemperature Andreev conductance reaches its optimal value $4e^2/h$ [13,17–20]. Thermal excitations can further activate the quasiparticle excitations from outside the pairing gap, giving rise to the Seebeck effect [21–23].

Charge transfer through multiterminal junctions is even more complex because of several possible transport channels. For instance, three-terminal setup with a single quantum dot on the interface of two normal electrodes and another

*Contact author: ggorski@ur.edu.pl

†Contact author: doman@kft.umcs.lublin.pl

superconducting electrode enables the single electron transfer (ET) as well as the direct (DAR) and/or crossed (CAR) Andreev reflections between the normal electrodes [20,24-30]. Under such circumstances, both the local and nonlocal transport coefficients can be measured [31]. It has been shown that when the crossed Andreev reflections prevail over the ballistic ET, the nonlocal conductance acquires negative values [10,16,29,32,33]. Furthermore, the temperature difference imposed in such a setup between the normal electrodes allows for separating the charge from the heat currents [34-37]. Interesting properties also occur in multiterminal geometries where the OD is between one normal and two superconducting electrodes, forming a Josephson-type junction [38-41]. The Kondo and Andreev effects there can be controlled by the phase difference (via magnetic field) between the superconducting electrodes.

In this paper we investigate signatures of the superconducting proximity effect appearing in the local and nonlocal transport properties of a three-terminal junction, considering two quantum dots in T-shaped geometry between two normal/ferromagnetic electrodes and the superconducting lead [42–47] (see Fig. 1). Bound states of the double dot molecules have so far been probed experimentally in two-terminal junctions using the scanning tunneling technique [48,49], as well as Josephson [50] and Andreev spectroscopy [51]. Here we consider a three-terminal configuration where the superconducting proximity effect is indirectly transmitted to one of the dots (QD₁) via the other one (QD₂); therefore, the interdot coupling plays a decisive role in affecting the local and nonlocal transport properties.

From numerical calculations we find that in the weak interdot coupling regime the interferometric features (Fanotype resonances) appear, whereas for tightly coupled dots we predict that the molecular bound states can induce negative conductance and lead to divergence of the Seebeck coefficient. These phenomena are caused solely by the Andreev

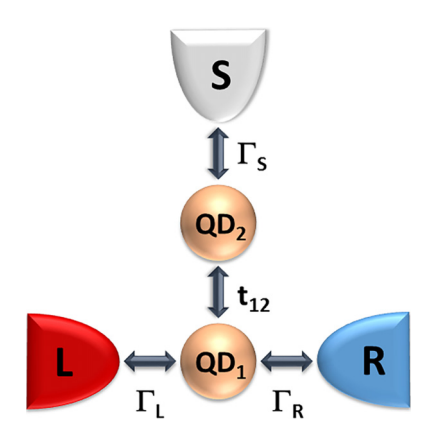


FIG. 1. Sketch of two quantum dots $(QD_1 \text{ and } QD_2)$ on the interface of a three-terminal junction. QD_1 is embedded between two normal/ferromagnetic leads (L and R) and is side attached to QD_2 , which is coupled to the superconductor (S).

scatterings. We investigate them and other related effects in the linear response limit, focusing on the deep subgap region.

This paper is organized as follows. We start by introducing the microscopic model (Sec. II A) and defining the transport coefficients (Secs. II B and II C). Next, we present our numerical results obtained for the normal (Sec. III) and ferromagnetic (Sec. IV) electrodes, examining the local and nonlocal properties of charge conductance and thermopower. In Sec. V we summarize the paper. The role of the Coulomb interaction is briefly discussed in Appendix A, and the influence of temperature on the transport coefficients of the polarized system is presented in Appendix B.

II. MODEL

We consider a three-terminal junction with two quantum dots in T-shaped geometry (Fig. 1), assuming the central quantum dot (QD_1) is weakly hybridized with the metallic (or ferromagnetic) electrodes and the second quantum dot (QD_2) is strongly coupled to an s-wave S lead. Such asymmetry of the couplings guarantees that the proximity effect induces narrow in-gap states at QD_2 which (through the interdot coupling) affect the spectrum of QD_1 , influencing the local and nonlocal transport properties of the junction.

A. Hamiltonian

Our hybrid structure can be described by the following Hamiltonian:

$$H = H_{DOD} + H_{N-QD1} + H_{S-QD2}.$$
 (1)

The double quantum dot term is given by

$$H_{\rm DQD} = \sum_{i\sigma} \varepsilon_{i\sigma} d^{\dagger}_{i\sigma} d_{i\sigma} + \sum_{\sigma} t_{12} (d^{\dagger}_{1\sigma} d_{2\sigma} + \text{H.c.}), \qquad (2)$$

where operators $d_{i\sigma}^{\dagger}(d_{i\sigma})$ create (annihilate) electrons on the ith quantum dot with spin σ and energy $\varepsilon_{i\sigma}$. For numerical computations, we assume the energy levels $\varepsilon_{i\sigma} = \varepsilon_i$ and the interdot hopping t_{12} are spin independent. This assumption is valid in the absence of external magnetic field; otherwise, the Zeeman splitting should be taken into account [52–54].

The term describing the normal/ferromagnetic leads and their hybridization with QD_1 can be expressed as

$$H_{\text{N-QD1}} = \sum_{\mathbf{k},\sigma,\alpha} (\varepsilon_{\mathbf{k}\alpha\sigma} - \mu_{\alpha}) c_{\mathbf{k}\alpha\sigma}^{\dagger} c_{\mathbf{k}\alpha\sigma} + \sum_{\mathbf{k},\sigma} (V_{\mathbf{k}\alpha\sigma} d_{1\sigma}^{\dagger} c_{\mathbf{k}\alpha\sigma} + \text{H.c.}),$$
(3)

where $c_{\mathbf{k}\alpha\sigma}^{\dagger}$ ($c_{\mathbf{k}\alpha\sigma}$) is the creation (annihilation) operator of a spin σ electron with momentum \mathbf{k} in the $\alpha=L$, R lead, $\varepsilon_{\mathbf{k}\alpha\sigma}$ is the kinetic energy, μ_{α} denotes the chemical potential, and $V_{k\alpha}$ is the hopping between external leads and QD₁. In the wide bandwidth limit, we can introduce the energy-independent tunnel couplings $\Gamma_{\alpha\sigma}=2\pi\sum_{k}|V_{k\alpha\sigma}|^2\delta(\omega-\varepsilon_{\mathbf{k}\alpha\sigma}+\mu_{\alpha\sigma})$. In Sec. IV we consider their spin-polarized versions, $\Gamma_{\alpha\sigma}=\Gamma_{\alpha}(1+\sigma p_{\alpha})$, assuming that $p_{L}=p_{R}\equiv p_{0}$.

The superconducting lead which is directly coupled to QD₂ will be treated within the BCS framework [18]:

$$H_{\text{S-QD2}} = \sum_{\mathbf{k},\sigma} (\varepsilon_{\mathbf{k}S\sigma} - \mu_S) c_{\mathbf{k}S\sigma}^{\dagger} c_{\mathbf{k}S\sigma}$$

$$+ \sum_{\mathbf{k}} \Delta (c_{\mathbf{k}S\downarrow} c_{-\mathbf{k}S\uparrow} + c_{-\mathbf{k}S\uparrow}^{\dagger} c_{\mathbf{k}S\downarrow}^{\dagger})$$

$$+ \sum_{\mathbf{k},\sigma} (V_{\mathbf{k}S\sigma} d_{2\sigma}^{\dagger} c_{\mathbf{k}S\sigma} + \text{H.c.}), \tag{4}$$

where, again, the operator $c_{\mathbf{k}S\sigma}^{\dagger}$ ($c_{\mathbf{k}S\sigma}$) refers to the creation (annihilation) of a spin σ electron with momentum \mathbf{k} , the kinetic energy $\varepsilon_{\mathbf{k}S\sigma}$ is measured with respect to the chemical potential μ_S , and Δ denotes the isotropic pairing gap. For convenience, we assume the superconducting lead is grounded, $\mu_S=0$.

In the absence of interdot coupling $(t_{12} = 0)$ and in the superconducting atomic limit $(\Delta \to \infty)$, the spectrum of QD_2 is characterized by a pair of Andreev bound states at energies $E_{A\pm} = \pm \sqrt{\varepsilon_2^2 + (\Gamma_S/2)^2}$, where $\Gamma_S = 2\pi \sum_{\mathbf{k}} |V_{\mathbf{k}S\sigma}|^2 \delta(\omega - \varepsilon_{\mathbf{k}S\sigma} + \mu_S)$ is the coupling strength between QD_2 and the superconducting lead. These Andreev states hybridize with the energy level of QD_1 through the interdot coupling t_{12} , leading to development of the molecular structure of the double quantum dot. For the uncorrelated setup we obtain the effective quasiparticle states at energies

$$\varepsilon_{\text{AD1}}^{\pm} = \pm \frac{1}{\sqrt{2}} \sqrt{A - \sqrt{A^2 - 4B}},$$
 (5)

$$\varepsilon_{\text{AD2}}^{\pm} = \pm \frac{1}{\sqrt{2}} \sqrt{A + \sqrt{A^2 - 4B}},$$
 (6)

where

$$A = \varepsilon_1^2 + E_{A+}^2 + 2t_{12}^2,\tag{7}$$

$$B = \left(\varepsilon_1 \varepsilon_2 - t_{12}^2\right)^2 + \left(\varepsilon_1 \Gamma_S / 2\right)^2. \tag{8}$$

The spectrum of the central quantum dot is presented in Secs. III and IV. For $t_{12} \rightarrow 0$ the quasiparticle energies simplify to $\varepsilon_{\rm AD1}^{\pm} \rightarrow \varepsilon_1$ and $\varepsilon_{\rm AD2}^{\pm} \rightarrow E_{A\pm}$, respectively.

The transport properties of this three-terminal system in-

The transport properties of this three-terminal system induced by the voltage applied to the normal leads $\mu_{\alpha} = eV_{\alpha}$ and/or by the temperature difference $T_L \neq T_R$ depend on the

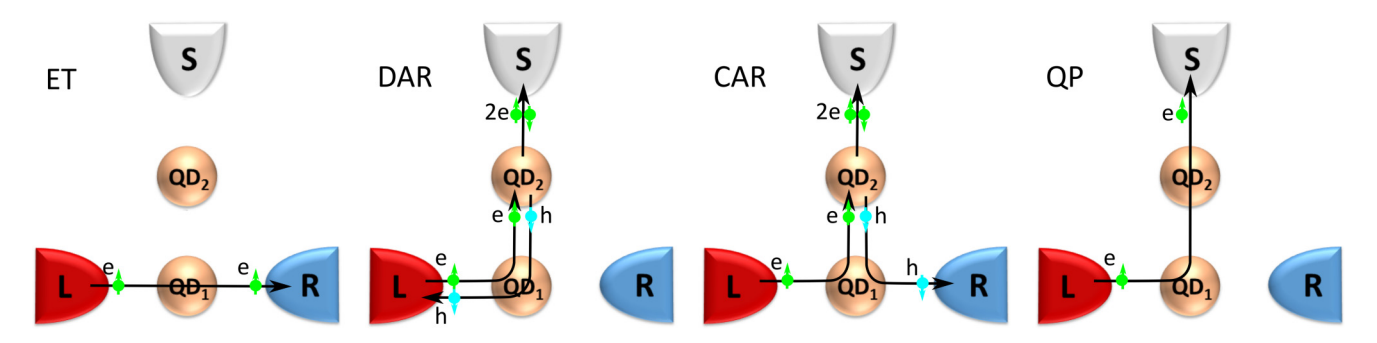


FIG. 2. Illustration of the charge transport processes in the three-terminal setup contributed by ballistic electron transfer (ET), direct Andreev reflection (DAR), crossed Andreev reflection (CAR), and quasiparticles tunneling (QP).

effective quasiparticle states of the quantum dots. In what follows we provide specific details concerning this issue.

B. Charge transport

Charge current from the Lth lead can be expressed by

$$J_{L\sigma} = -e \frac{d}{dt} \left\langle \sum_{\mathbf{k}} c_{\mathbf{k}L\sigma}^{\dagger} c_{\mathbf{k}L\sigma} \right\rangle$$
$$= \frac{ie}{\hbar} \left\langle \sum_{\mathbf{k}} [c_{\mathbf{k}L\sigma}^{\dagger} c_{\mathbf{k}L\sigma}, H]_{-} \right\rangle. \tag{9}$$

From a straightforward analysis we obtain

$$J_{L\sigma} = \frac{2e}{\hbar} \sum_{\mathbf{k}} \text{Re}[V_{\mathbf{k}L\sigma} \mathcal{G}^{<}_{1\sigma,\mathbf{k}L\sigma}(t,t)], \tag{10}$$

where $\mathcal{G}^{<}_{1\sigma,\mathbf{k}L\sigma}(t,t')=i\langle c^{\dagger}_{\mathbf{k}L\sigma}(t')d_{1\sigma}(t)\rangle$ is the lesser Green's function. Introducing the Fourier transform and following the

procedure formulated by Haug and Jauho [55], we can express

$$J_{L\sigma} \text{ as } J_{L\sigma} = -\frac{2e}{h} \frac{\Gamma_{L\sigma}}{2} \int d\omega \text{Im} \Big[2f_{L\sigma} \langle \langle d_{1\sigma} | d_{1\sigma}^{\dagger} \rangle \rangle_{\omega}^{r} + \langle \langle d_{1\sigma} | d_{1\sigma}^{\dagger} \rangle \rangle_{\omega}^{\varsigma} \Big],$$

$$(11)$$

where $f_{\alpha\sigma} = \{\exp[(\omega - \mu_{\alpha\sigma})/k_B T_{\alpha}] + 1\}^{-1}$ is the Fermi-Dirac distribution function.

The retarded Green's function $\langle\langle d_{1\sigma}|d_{1\sigma}^{\dagger}\rangle\rangle_{\omega}^{r}$ can be determined from the equation of motion

$$\omega \langle \langle \Psi_i | \Psi_j \rangle \rangle_{\omega}^r = \langle [\Psi_i, \Psi_j]_+ \rangle + \langle \langle [\Psi_i, H]_- | \Psi_j \rangle \rangle_{\omega}^r \quad (12)$$

for the matrix Green's function $\hat{\mathcal{G}}^r(\omega) = \langle\langle\hat{\Psi}|\hat{\Psi}^\dagger\rangle\rangle_\omega^r$, which is defined in the Nambu spinor representation $\hat{\Psi}^\dagger=(d_{1\uparrow}^\dagger,d_{1\downarrow},d_{2\uparrow}^\dagger,d_{2\downarrow})$. On the other hand, the lesser Green's function obeys the Keldysh equation [55]

$$\hat{\mathcal{G}}^{<}(\omega) = \hat{\mathcal{G}}^{r}(\omega)\hat{\Sigma}^{<}(\omega)\hat{\mathcal{G}}^{a}(\omega), \tag{13}$$

where $\hat{\Sigma}^{<}(\omega)$ denotes the lesser self-energy matrix.

The lesser self-energy matrix, appearing in Eq. (13), can be expressed as

$$\hat{\Sigma}^{<}(\omega) = -i \begin{pmatrix} \Gamma_{L\uparrow} f_{L\uparrow} + \Gamma_{R\uparrow} f_{R\uparrow} & 0 & 0 & 0\\ 0 & \Gamma_{L\downarrow} \tilde{f}_{L\downarrow} + \Gamma_{R\downarrow} \tilde{f}_{R\downarrow} & 0 & 0\\ 0 & 0 & \Gamma_{S} \beta(\omega) f_{S} & \Gamma_{S} \beta(\omega) \frac{\Delta}{\omega} f_{S}\\ 0 & 0 & \Gamma_{S} \beta(\omega) \frac{\Delta^{*}}{\omega} f_{S} & \Gamma_{S} \beta(\omega) f_{S} \end{pmatrix}, \tag{14}$$

where $\tilde{f}_{\alpha\sigma} = \{\exp[(\omega + \mu_{\alpha\sigma})/k_BT_{\alpha}] + 1\}^{-1}$ is the distribution function for holes and $\beta(\omega) = \frac{|\omega|\Theta(|\omega|-\Delta)}{\sqrt{\omega^2-\Delta^2}} - \frac{i\omega\Theta(\Delta-|\omega|)}{\sqrt{\Delta^2-\omega^2}}$. For the uncorrelated setup (neglecting the Coulomb repulsion on both quantum dots) we obtain [18]

$$\hat{\mathcal{G}}^{r(a)}(\omega) = \begin{pmatrix} \omega - \epsilon_{1\uparrow} \pm i\frac{\Gamma_{N\uparrow}}{2} & 0 & t_{12} & 0 \\ 0 & \omega + \epsilon_{1\downarrow} \pm i\frac{\Gamma_{N\downarrow}}{2} & 0 & -t_{12} \\ t_{12} & 0 & \omega - \epsilon_{2\uparrow} \pm i\frac{\Gamma_{S}}{2}\beta(\omega) & \pm i\frac{\Gamma_{S}}{2}\beta(\omega)\frac{\Delta}{\omega} \\ 0 & -t_{12} & \pm i\frac{\Gamma_{S}}{2}\beta(\omega)\frac{\Delta^{*}}{\omega} & \omega + \epsilon_{2\downarrow} \pm i\frac{\Gamma_{S}}{2}\beta(\omega) \end{pmatrix}^{-1}.$$
(15)

Using this formalism, we can represent the charge current (11) by contributions from the ballistic ET, DAR, CAR, and the quasiparticle flow (QP):

$$J_{L\sigma} = J_{L\sigma}^{\text{ET}} + J_{L\sigma}^{\text{DAR}} + J_{L\sigma}^{\text{CAR}} + J_{L\sigma}^{\text{QP}}.$$
 (16)

These transport channels are graphically displayed in Fig. 2. The ballistic transfer of electrons from the *L* to *R* lead through

QD₁ can be expressed as

$$J_{L\sigma}^{\rm ET} = \frac{e}{h} \int d\omega T_{\sigma}^{\rm ET}(\omega) [f_{L\sigma}(\omega) - f_{R\sigma}(\omega)], \tag{17}$$

where the tunneling transmittance is given by

$$T_{\sigma}^{\rm ET}(\omega) = \Gamma_{L\sigma} \Gamma_{R\sigma} \left| \langle \langle d_{1\sigma} | d_{1\sigma}^{\dagger} \rangle \rangle_{\omega}^{r} \right|^{2}. \tag{18}$$

The DAR describes the conversion of the electron from the Lth lead to the local pair at QD_2 , followed by its injection into the superconductor, while a hole of opposite spin is scattered back to the same electrode. This current is given by

$$J_{L\sigma}^{\rm DAR} = \frac{e}{\hbar} \int d\omega T_{\sigma}^{\rm DAR}(\omega) [f_{L\sigma}(\omega) - \tilde{f}_{L-\sigma}(\omega)], \quad (19)$$

with the transmittance

$$T_{\sigma}^{\text{DAR}}(\omega) = \Gamma_{L\sigma} \Gamma_{L-\sigma} \left| \left\langle \left\langle d_{1\sigma} | d_{1-\sigma} \right\rangle \right\rangle_{\omega}^{r} \right|^{2}. \tag{20}$$

The crossed Andreev reflection process is similar to DAR, except that it injects a hole into the *R*th lead:

$$J_{L\sigma}^{\text{CAR}} = \frac{e}{\hbar} \int d\omega T_{\sigma}^{\text{CAR}}(\omega) [f_{L\sigma}(\omega) - \tilde{f}_{R-\sigma}(\omega)], \quad (21)$$

where the corresponding transmittance

$$T_{\sigma}^{\text{CAR}}(\omega) = \Gamma_{L\sigma} \Gamma_{R-\sigma} \left| \langle \langle d_{1\sigma} | d_{1-\sigma} \rangle \rangle_{\omega}^{r} \right|^{2}. \tag{22}$$

The last term in Eq. (16) describes the single electron transfer from the Lth lead to a continuum outside the pairing gap of the superconductor. This quasiparticle current is given as

$$J_{L\sigma}^{\rm QP} = \frac{e}{\hbar} \int d\omega T_{\sigma}^{\rm QP}(\omega) [f_{L\sigma}(\omega) - f_{S\sigma}(\omega)], \qquad (23)$$

with the transmittance [17]

$$T_{\sigma}^{\text{QP}}(\omega) = \text{Re}[\beta(\omega)] \Gamma_{L\sigma} \Gamma_{S\sigma} \left(\left| \left\langle \left\langle d_{1\sigma} | d_{2\sigma}^{\dagger} \right\rangle \right\rangle_{\omega}^{r} \right|^{2} \right. \\ \left. + \left| \left\langle \left\langle d_{1\sigma} | d_{2-\sigma} \right\rangle \right\rangle_{\omega}^{r} \right|^{2} \right. \\ \left. + 2 \frac{\Delta}{\omega} \text{Re} \left[\left\langle \left\langle d_{1\sigma} | d_{2\sigma}^{\dagger} \right\rangle \right\rangle_{\omega}^{r} \left\langle \left\langle d_{2-\sigma}^{\dagger} | d_{1\sigma}^{\dagger} \right\rangle \right\rangle_{\omega}^{a} \right] \right). (24)$$

We note that Eq. (25) depends on $\text{Re}[\beta(\omega)]$, whose non-vanishing value $T_{\sigma}^{\text{QP}}(\omega)$ occurs solely for $|\omega| > \Delta$. This current J^{QP} is hence meaningful only for a sufficiently large voltage, $|eV_L| > \Delta$, and/or at sufficiently large temperatures, $k_B T \geqslant \Delta$.

In an analogous way we can express the charge current from the Rth electrode J_R by swapping the indices $L \leftrightarrow R$.

C. Linear response limit

In the present work we shall focus on the low-temperature limit $T \ll T_c$ (where T_c denotes the superconducting critical temperature) and consider infinitesimally small perturbations, $\mu_{\alpha} = e \delta V_{\alpha}$ and $T_{L,R} = T_S + \delta T_{L,R}$. The charge current from

the Lth lead then simplifies to

$$J_{L\sigma} = D_{\sigma\mu}^{\text{ET}}(e\delta V_L - e\delta V_R) + 2D_{\sigma\mu}^{\text{DAR}}e\delta V_L$$

+ $D_{\sigma\mu}^{\text{CAR}}(e\delta V_L + e\delta V_R) + D_{\sigma\mu}^{\text{QP}}e\delta V_L$
+ $D_{\sigma T}^{\text{QP}}\delta T_L + \left(D_{\sigma T}^{\text{ET}} + D_{\sigma T}^{\text{CAR}}\right)(\delta T_L - \delta T_R), \quad (25)$

where the coefficients

$$D_{\sigma\mu}^{\kappa} = \frac{e}{\hbar} \int d\omega T_{\sigma}^{\kappa}(\omega) \left[-\frac{\partial f}{\partial \omega} \right], \tag{26}$$

$$D_{\sigma T}^{\kappa} = \frac{e}{\hbar T} \int d\omega \omega T_{\sigma}^{\kappa}(\omega) \left[-\frac{\partial f}{\partial \omega} \right]$$
 (27)

refer to $\kappa = \{ET, DAR, CAR, QP\}$ transport channels.

Let us now define the local conductance $G_{\alpha\alpha\sigma} = \frac{dJ_{\alpha\sigma}}{dV_{\alpha}}|_{\delta T=0}$ and nonlocal electrical conductance $G_{\alpha\beta\sigma} = -\frac{dJ_{\alpha\sigma}}{dV_{\beta}}|_{\delta T=0}$, where $\alpha \neq \beta$ [24,28,31]. Equation (16) implies that the local conductance is contributed by all transport channels,

$$G_{LL\sigma} = G_{\sigma}^{\text{ET}} + 2G_{\sigma}^{\text{DAR}} + G_{\sigma}^{\text{CAR}} + G_{\sigma}^{\text{QP}}, \tag{28}$$

whereas the nonlocal conductance is given by a difference in the electron transfer and the crossed Andreev reflection,

$$G_{RL\sigma} = G_{\sigma}^{\rm ET} - G_{\sigma}^{\rm CAR},\tag{29}$$

where $G^{\kappa}_{\sigma} = e D^{\kappa}_{\sigma\mu}$. We clearly notice that the nonlocal conductance (29) takes either positive or negative values, depending on the dominant transport channel. In particular, it will be negative when the superconducting proximity effect plays a major role, promoting the Andreev scattering over the single electron ballistic transfer.

At zero temperature the transport coefficients $D^{\kappa}_{\sigma\mu}$ of our uncorrelated setup simplify to

$$D_{\sigma\mu}^{\text{ET}} = \frac{e}{\hbar} \frac{\Gamma_{L\sigma} \Gamma_{R\sigma} \left[\left(\varepsilon_2 t_{12}^2 - \varepsilon_1 E_{A+}^2 \right)^2 + \frac{\Gamma_N^2}{4} E_{A+}^4 \right]}{\left[\frac{\Gamma_N^2}{4} E_{A+}^2 + B \right]^2}, \tag{30}$$

$$D_{\sigma\mu}^{\text{DAR}} = \frac{e}{\hbar} \frac{\Gamma_{L\sigma} \Gamma_{L-\sigma} \frac{\Gamma_s^2}{4} t_{12}^4}{\left[\frac{\Gamma_N^2}{4} E_{A\perp}^2 + B\right]^2},$$
 (31)

$$D_{\sigma\mu}^{\text{CAR}} = \frac{e}{\hbar} \frac{\Gamma_{L\sigma} \Gamma_{R-\sigma} \frac{\Gamma_s^2}{4} t_{12}^4}{\left[\frac{\Gamma_N^2}{4} E_{A+}^2 + B\right]^2},$$
 (32)

and

$$D_{\sigma\mu}^{\rm QP} = 0. \tag{33}$$

Under such circumstances, the coefficients $D_{\sigma\mu}^{\kappa}$ do not depend on the pairing gap of superconductor.

From Eqs. (30)–(33) we can derive explicit expressions for the local and nonlocal electrical conductances:

$$G_{LL\sigma} = \frac{e^2}{\hbar} \frac{\Gamma_{L\sigma} \Gamma_{R\sigma} \left[\left(\varepsilon_2 t_{12}^2 - \varepsilon_1 E_{A+}^2 \right)^2 + \frac{\Gamma_N^2}{4} E_{A+}^4 \right] + 2\Gamma_{L\sigma} \Gamma_{L-\sigma} \frac{\Gamma_N^2}{4} t_{12}^4 + \Gamma_{L\sigma} \Gamma_{R-\sigma} \frac{\Gamma_N^2}{4} t_{12}^4}{\left[\frac{\Gamma_N^2}{4} E_{A+}^2 + B \right]^2},$$
(34)

$$G_{RL\sigma} = \frac{e^2}{\hbar} \frac{\Gamma_{L\sigma} \Gamma_{R\sigma} \left[\left(\varepsilon_2 t_{12}^2 - \varepsilon_1 E_{A+}^2 \right)^2 + \frac{\Gamma_N^2}{4} E_{A+}^4 \right] - \Gamma_{L\sigma} \Gamma_{R-\sigma} \frac{\Gamma_N^2}{4} t_{12}^4}{\left[\frac{\Gamma_N^2}{4} E_{A+}^2 + B \right]^2}.$$
 (35)

For the setup with ferromagnetic electrodes the conductance depends on spin, $G_{LL\uparrow} \neq G_{LL\downarrow}$. Under such conditions the local and nonlocal conductances are

$$G_{LL} = \sum_{\sigma} G_{LL\sigma}, \quad G_{RL} = \sum_{\sigma} G_{RL\sigma}.$$
 (36)

We can also introduce their spin-polarized versions

$$P_{G_{LL}} = \frac{G_{LL\uparrow} - G_{LL\downarrow}}{G_{LL}}, \quad P_{G_{RL}} = \frac{G_{RL\uparrow} - G_{RL\downarrow}}{G_{RL}}.$$
 (37)

In a similar way, for the temperature gradient ΔT_{α} we define the local, $S_{\alpha\alpha\sigma} = -\frac{dV_{\alpha}}{dT_{\alpha}}|_{J_{\gamma\sigma}=0}$, and nonlocal, $S_{\alpha\beta\sigma} = -\frac{dV_{\alpha}}{dT_{\beta}}|_{J_{\gamma\sigma}=0}$, Seebeck coefficients, where voltage V_{α} compensates the current induced by temperature gradient, $J_{\gamma\sigma}=0$. For an infinitesimally small temperature difference the thermopower can be expressed by

$$S_{LL\sigma} = \frac{D_{\sigma T}^{\rm ET} + D_{\sigma T}^{\rm CAR} + D_{\sigma T}^{\rm QP}}{G_{LL\sigma}},$$
 (38)

$$S_{RL\sigma} = -\frac{D_{\sigma T}^{\text{ET}} + D_{\sigma T}^{\text{CAR}} + D_{\sigma T}^{\text{QP}}}{G_{RL\sigma}}.$$
 (39)

In the case of ferromagnetic electrodes $S_{LL\uparrow} \neq S_{LL\downarrow}$; therefore, we can consider the average Seebeck coefficients

$$S_{LL} = \frac{S_{LL\uparrow} + S_{LL\downarrow}}{2}, \quad S_{RL} = \frac{S_{RL\uparrow} + S_{RL\downarrow}}{2}$$
 (40)

and their spin-resolved counterparts [56,57]

$$S_{LL}^{S} = \frac{S_{LL\uparrow} - S_{LL\downarrow}}{2}, \ S_{RL}^{S} = \frac{S_{RL\uparrow} - S_{RL\downarrow}}{2}.$$
 (41)

In the following sections we present the characteristic properties obtained numerically for the local and nonlocal transport coefficients of a three-terminal setup with normal and ferromagnetic leads.

III. SETUP WITH NORMAL ELECTRODES

Let us start by considering the spin-resolved spectrum of the central quantum dot (QD_1) and then discuss its influence on the transport properties of our system. For computations, we treat $\Gamma_N = \Gamma_L + \Gamma_R \equiv 1$ as a convenient energy unit and assume strong coupling to the superconductor $\Gamma_S = 2\Gamma_N$ to obtain well-pronounced signatures of the quasiparticle states in the spectra of both quantum dots.

Equations (34) and (35) show that at zero temperature the local and nonlocal conductances do not depend on the pairing gap of the superconducting lead. For this reason, to simplify our study and reduce the number of model parameters, we restrict ourselves to the superconducting atomic limit approach ($\Delta \to \infty$). This approach is valid when the energies ε_i are deep inside the pairing gap of the superconductor Δ and temperature is safely smaller than T_c . Otherwise, the continuum electronic states from outside the pairing will play important role.

A. Quasiparticle spectrum

We first analyze the quasiparticles of the quantum dots, depending on the interdot coupling and their energy levels.

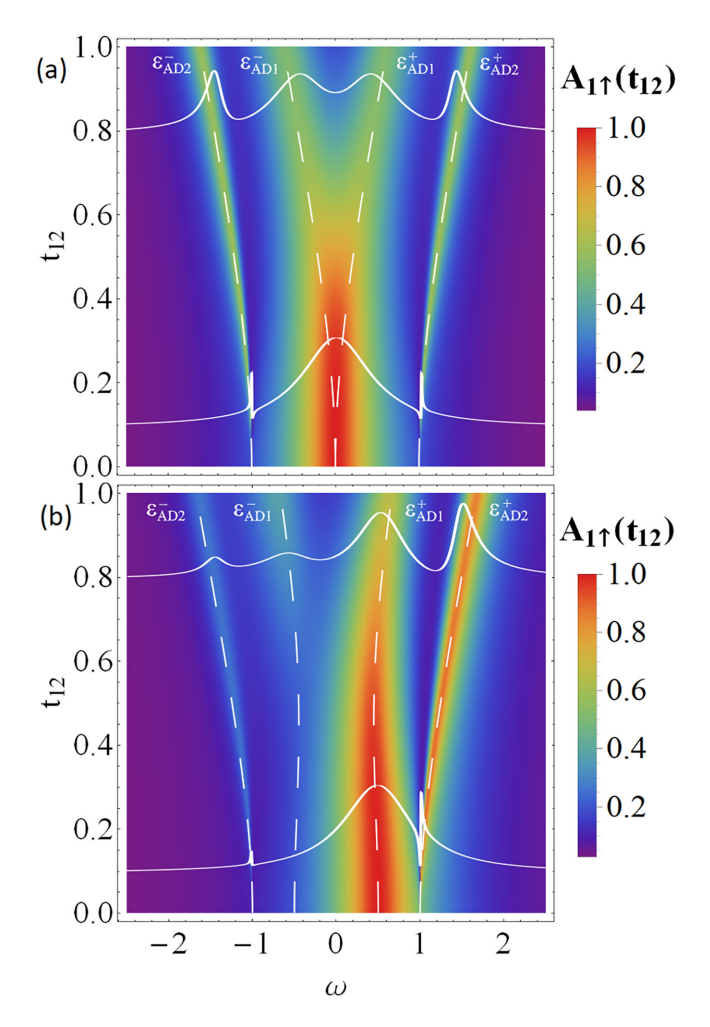


FIG. 3. The spectral function $A_{1\uparrow}(\omega)$ of QD₁ as a function of the interdot coupling t_{12} obtained for (a) $\varepsilon_1 = 0$ and (b) $\varepsilon_1 = 0.5$ using the model parameters $\varepsilon_2 = 0$, $\Gamma_S = 2$, $\Gamma_L = \Gamma_R = 0.5$, $k_BT = 0$, and $p_0 = 0$. White solid lines display the profile of the spectral function in the weak ($t_{12} = 0.1$) and strong ($t_{12} = 0.8$) coupling limits. The quasiparticle energies $\varepsilon_{\text{AD1}}^{\pm}$ and $\varepsilon_{\text{AD2}}^{\pm}$, given by Eqs. (5) and (6), are marked by white dashed lines.

Let us consider the spectral function

$$A_{1\sigma}(\omega) = -\frac{\Gamma_N}{2} \text{Im} \langle \langle d_{1\sigma}; d_{1\sigma}^{\dagger} \rangle \rangle_{\omega}^r$$
 (42)

of the central quantum dot (normalized here by the factor $\pi\Gamma_N/2$ to obtain dimensionless values). This quantum dot affects all four transport processes in our setup (displayed in Fig. 2). For the nonmagnetic L and R leads, this function (42) is spin independent.

In Fig. 3 we present the spectrum of \uparrow -spin electrons of QD₁ obtained for the energy levels $\varepsilon_1=0$ [Fig. 3(a)] and $\varepsilon_1=0.5$ [Fig. 3(b)]. For isolated quantum dots, $t_{12}=0$, the spectral function of QD₁ takes the well-known Lorentzian shape centered near $\omega=\varepsilon_1$. For finite interdot coupling, $t_{12}\neq 0$, we can observe two different effects, depending on the ratio t_{12}/Γ_N [47]. In the weak coupling limit, $t_{12}/\Gamma_N < 0.5$, the interferometric (Fano-type) structures emerge at $\omega=E_{A\pm}$. In the strong coupling limit, $t_{12}/\Gamma_N\geqslant 0.5$, we observe the development of a molecular quasiparticle spectrum

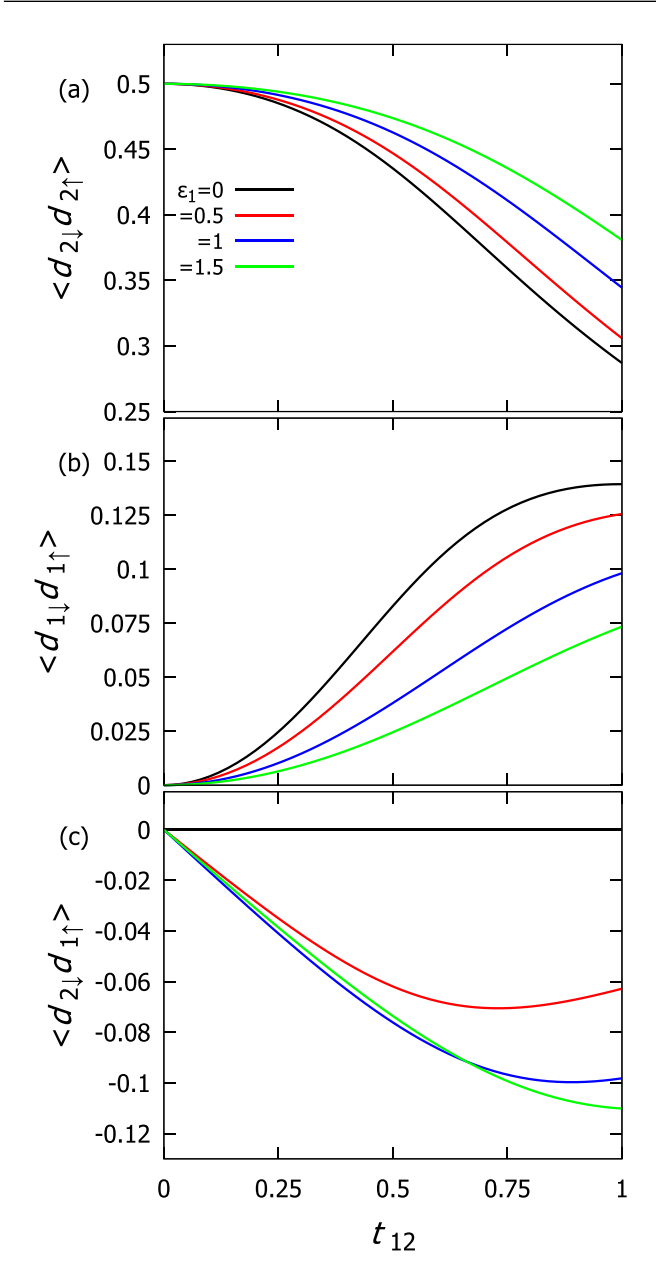


FIG. 4. The (a) and (b) local and (c) nonlocal electron pairings plotted vs the interdot coupling t_{12} for several energy levels ε_1 , as indicated. Computations are done for the following set of model parameters: $\varepsilon_2 = 0$, $\Gamma_S = 2$, $\Gamma_L = \Gamma_R = 0.5$, T = 0, and $p_0 = 0$.

characterized by four peaks (two pairs symmetrically placed around the Fermi level). This molecular structure is induced by leakage of the electron pairs from the superconducting lead onto both quantum dots. To support this claim we show in Fig. 4 the variation of the on-dot and interdot pairings:

$$\langle d_{i\downarrow}d_{j\uparrow}\rangle = \frac{-1}{\pi} \int_{-\infty}^{\infty} \operatorname{Im}\langle\langle d_{j\uparrow}; d_{i\downarrow}\rangle\rangle_{\omega}^{r} \frac{1}{1 + e^{\omega/k_{B}T}} d\omega. \tag{43}$$

Figure 4 shows the variation of the local and nonlocal pairings with respect to t_{12} for several values of ε_1 . With increasing t_{12} the local pairing induced in QD₁ is gradually amplified at the expense of a partial weakening of the electron pairing in QD₂. For the fully symmetric case, $\varepsilon_1 = 0 = \varepsilon_2$,

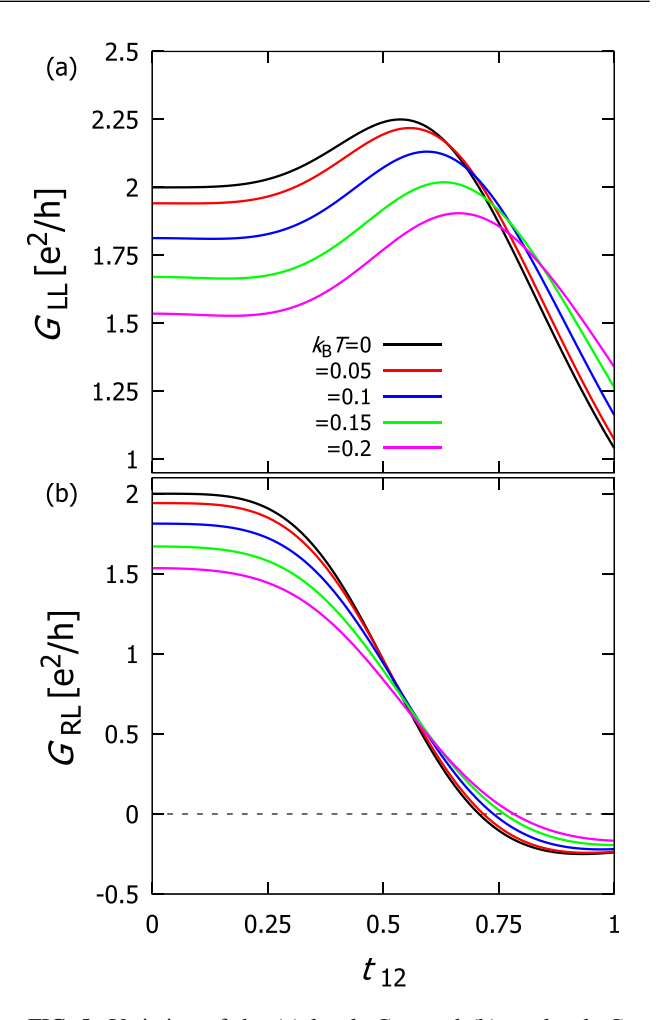


FIG. 5. Variation of the (a) local, G_{LL} , and (b) nonlocal, G_{RL} , conductances versus the interdot coupling t_{12} for several temperatures, as indicated. Results are obtained for the model parameters $\varepsilon_1 = \varepsilon_2 = 0$, $\Gamma_S = 2$, $\Gamma_L = \Gamma_R = 0.5$, and $p_0 = 0$.

the nonlocal singlet pairing $\langle d_{2\downarrow}d_{1\uparrow}\rangle$ is completely absent. It emerges solely in the asymmetric case, $\varepsilon_1 \neq \varepsilon_2$, yet is an order of magnitude smaller in comparison to the local pairings. Of particular importance for the charge transport properties (discussed in next section) is $\langle d_{1\downarrow}d_{1\uparrow}\rangle$ because it controls the efficiency of the Andreev scattering processes.

B. Zero-bias conductance

Electron pairing induced in QD₂ by the proximity effect and subsequently transmitted to the central quantum dot leads to characteristic features in the local and nonlocal transport properties. We discuss their signatures in the conductance and analyze their qualitative changes with varying interdot coupling (Fig. 5).

When the quantum dots are separated, $t_{12}=0$, the conductance is contributed only by the ballistic electron transport (30), which at zero temperature takes a unitary limit value of $2e^2/h$. By coupling these dots, $t_{12} \neq 0$, we observe a slight reduction of $G^{\rm ET}$ (due to the suppression of the quasiparticle state at $\omega=0$), while an additional contribution comes from the Andreev channel $G^{\rm DAR(CAR)}$, enhancing the total conductance above its initial value of $2e^2/h$. In the strong

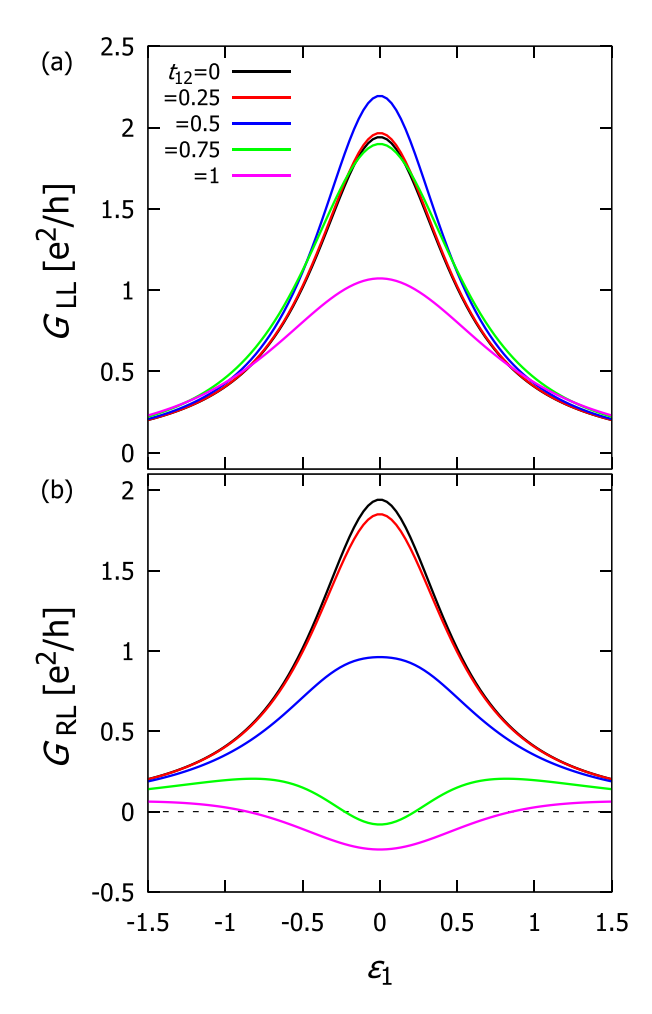


FIG. 6. (a) Local, G_{LL} , and (b) nonlocal, G_{RL} , total zero-bias conductivities with respect to the QD₁ energy for different values of t_{12} . Other parameters are $\varepsilon_2 = 0$, $\Gamma_S = 2$, $\Gamma_L = \Gamma_R = 0.5$, $p_0 = 0$, and $k_B T = 0.05$.

interdot coupling limit, $t_{12} > 0.5$, the local conductance is substantially suppressed because the quasiparticle state, initially existing at $\omega = \varepsilon_1$, gradually evolves into the molecular structure represented by four peaks (see Fig. 3).

In contrast to G_{LL} , the nonlocal conductance turns out to be a very sensitive probe of the competition between the crossed Andreev reflections and the ballistic electron transfers. This property can be inferred from Eq. (29) and can be observed for arbitrary interdot couplings t_{12} . Ultimately, for the tightly coupled quantum dots ($t_{12} \ge 0.75$) the sign-reversal of G_{RL} occurs in analogy to the results previously obtained for the three-terminal structure with a single quantum dot, both in the uncorrelated [58] and strongly correlated [20] cases.

The energy levels also have some influence on the efficiency of the superconducting proximity effect. Optimal conditions for the on-dot pairing induced in QD₁ occur in the symmetric case, $\varepsilon_{1,2} = 0$ [black line in Fig. 4(b)]. Under such circumstances the local conductance G_{LL} reaches its maximum at $t_{12} \approx 0.5$ [see Fig. 6(a)]. Far away from the symmetric case the on-dot pairing (43) becomes residual; therefore, the local conductance practically does not vary against ε_1 . This

behavior is evident from Fig. 6(b), which shows that negative values of the nonlocal conductance (where the crossed Andreev reflections dominate over ballistic transfer) are realized in the strong interdot coupling limit solely when $|\varepsilon_1| < 0.75$.

The energy levels (tunable by external gate potentials) along with the interdot coupling (transmitting electron pairing from QD_2 to QD_1) thus control the relationship between the single particle electron transfer and the anomalous electron-to-hole scattering processes.

C. Thermopower

We now study how different transport channels affect the thermoelectric properties. Usually, in bulk materials the sign of the Seebeck coefficient reverses during the changeover from electron- to hole-dominated transport regions. The same behavior occurs in two-terminal metallic junctions with a single quantum dot, where the thermopower takes sawtooth shape as a function of the energy level [57,59]. In two-terminal nanostructures with a quantum dot between a normal and superconducting electrode, the nonvanishing value of the Seebeck coefficient is obtained either at high temperatures or in the presence of the Zeeman splitting [21].

We can identify the particle and hole dominant regions of our three-terminal setup by inspecting the local Seebeck coefficient and can distinguish between the ballistic and Andreev-type contributions using the nonlocal coefficient. Figure 7 shows the variation of the local S_{LL} and S_{RL} Seebeck coefficients with respect to the QD₁ energy level obtained for several values of t_{12} . In analogy with two-terminal junctions, the local Seebeck coefficient has a negative sign for $\varepsilon_1 < 0$ and is positive for $\varepsilon_1 > 0$. The interdot coupling t_{12} causes only a flattening of its sawtooth shape.

The nonlocal Seebeck coefficient, on the other hand, is very sensitive to t_{12} . For small t_{12} the nonlocal S_{RL} has a shape typical for a metallic dot, i.e., $S_{RL} > 0$ for $\varepsilon_1 < 0$ and $S_{RL} < 0$ for $\varepsilon_1 > 0$ (see, e.g., [26,57]). For the strong interdot coupling limit (when the molecular Andreev bound states are formed on QD₁ and QD₂) we observe divergence and sign reversal of S_{RL} . This behavior is typical for the superconducting-proximity-effect regime, where $S_{RL} < 0$ for $\varepsilon_1 < 0$ and $S_{RL} > 0$ for $\varepsilon_1 > 0$ (see Refs. [28,60]).

This divergence point corresponds to the changeover from the thermoelectricity dominated by the ballistic channel to the region dominated by the crossed Andreev reflections. This information is thus complementary to that for the local Seebeck coefficient.

IV. SETUP WITH FERROMAGNETIC LEADS

We now consider the influence of electrode polarization p_0 on the properties of our system. Magnetically polarized electrodes can be expected to induce spin-dependent features, analogous to those due to Zeeman splitting. Since magnetism and superconductivity compete with each other, it is therefore important to analyze how they show up in the quasiparticle spectra of QD_1 and how they affect the transport properties of our superconducting nanostructure.

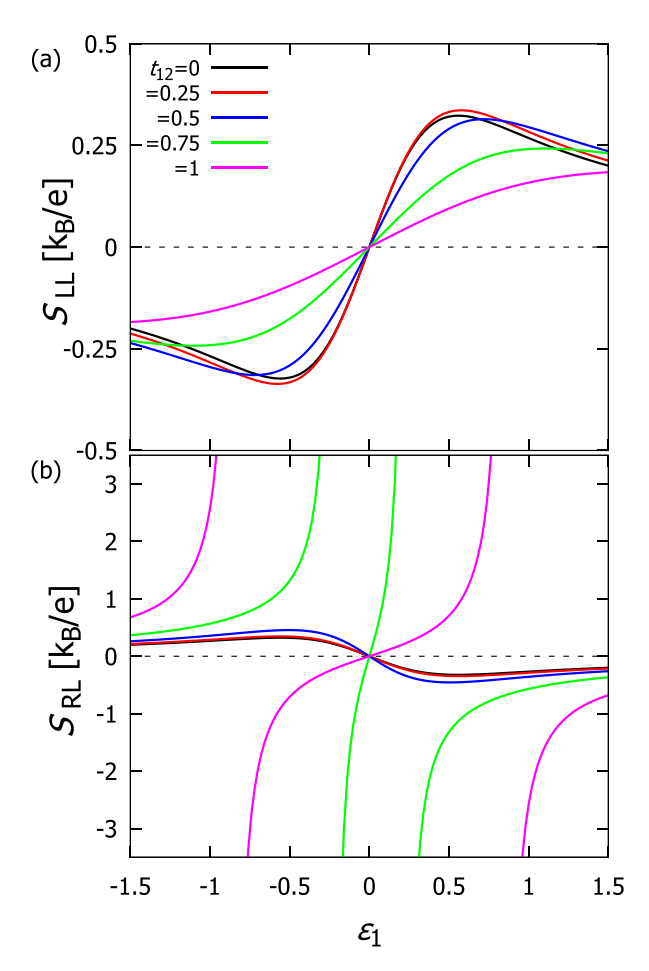


FIG. 7. (a) Local, S_{LL} , and (b) nonlocal, S_{RL} , thermopowers with respect to the QD₁ energy for different values of t_{12} , using the model parameters $\varepsilon_2=0$, $\Gamma_S=2$, $\Gamma_L=\Gamma_R=0.5$, $p_0=0$, and $k_BT=0.05$.

A. Polarized spectrum

To proceed, let us analyze the influence of the polarization on the quasiparticle spectra of the quantum dots, focusing on QD₁ because of its crucial role for the transport properties. Figure 8 shows the variation of the spin-resolved spectrum of QD₁ with respect to p_0 obtained for $\varepsilon_1 = 0 = \varepsilon_2$ and interdot coupling $t_{12} = 0.5$, where we can clearly resolve the quasiparticle states of odd and even parity. For $p_0 = 0$ the spectrum consists of the central peak at ε_1 and two Fano-type resonances near $\pm \Gamma_S/2$ driven by the superconducting proximity effect. With increasing polarization the spectral function of the spin-↑ electrons absorbs more and more spectral weight, and simultaneously, the central peak gradually splits. In contrast, the outer resonances do not change position, proving that they correspond to the spinless BCS-type states $u^2|0\rangle \pm v^2|\uparrow\downarrow\rangle$. As far as the spectrum of the spin-↓ electrons is concerned, the polarization of external leads depletes its spectral weight. Both these phenomena have a strong effect on the transport properties, especially their spin-sensitive versions.

B. Conductance of the polarized system

Polarization affects the charge transport in both the ballistic channel and Andreev-type processes. In the first case

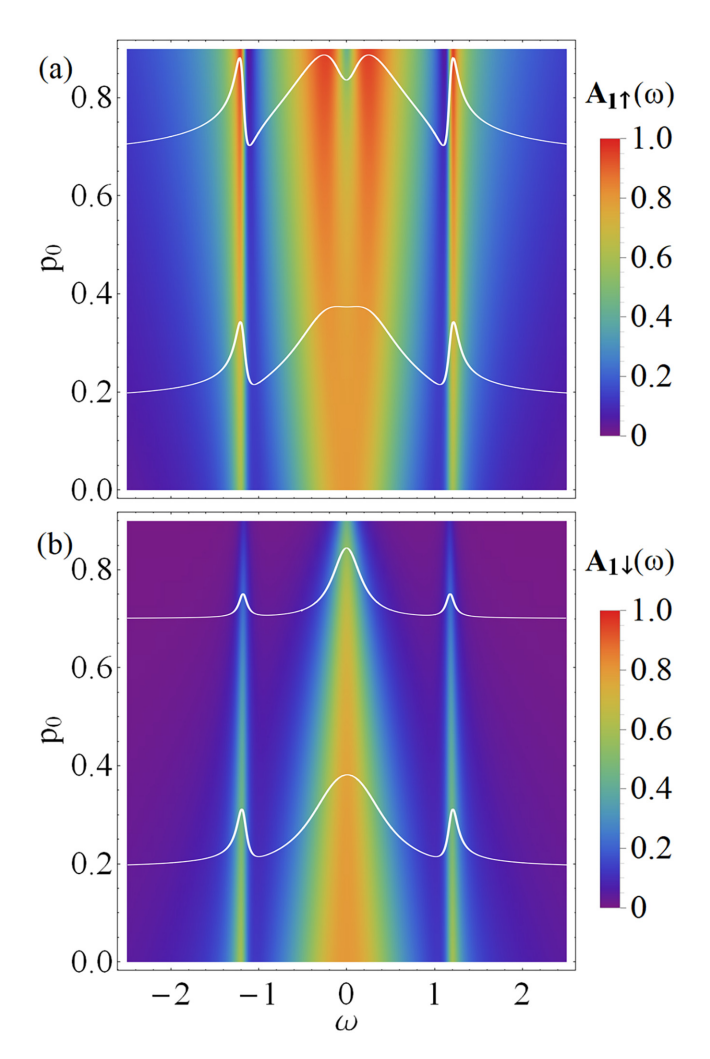


FIG. 8. The normalized spectral function $A_{1\sigma}(\omega)$ of QD₁ as a function of the polarization parameter p_0 . Numerical results are obtained for $\varepsilon_1 = \varepsilon_2 = 0$, $\Gamma_S = 2$, $\Gamma_L = \Gamma_R = 0.5$, $t_{12} = 0.5$, and T = 0. White lines show the profiles of the spectral function of the weakly ($p_0 = 0.2$) and strongly ($p_0 = 0.7$) polarized systems.

its influence comes predominantly from renormalization of the low-energy spectral functions $A_{1\sigma}(\omega=0)$, whereas the electron-to-hole scatterings are sensitive to the modified electron pairing on QD₁. Evolution of the quasiparticle spectrum (discussed in Sec. IV A) thus suggests a detrimental influence of the polarization on the differential conductance.

Figure 9 shows the variation of the local conductance G_{LL} [Fig. 9(a)] and its polarization $P_{G_{LL}}$ [Fig. 9(b)] with respect to the energy level ε_1 for several t_{12} and p_0 . As expected, for all values of the interdot coupling, the local conductance is suppressed by p_0 . The polarized conductance [Fig. 9(b)] proves that the spin-resolved ballistic channel is mostly affected when ε_1 is distant from the symmetry point. The Andreev channels (simultaneously involving both spin components) are responsible for suppressing the local conductance when $\varepsilon_1 \sim 0$.

Figure 10(a) presents the nonlocal conductance G_{RL} obtained for different values of t_{12} and p_0 . Again, we observe that for small $|\varepsilon_1|$ the polarization p_0 suppresses mainly the crossed Andreev reflections. The polarized nonlocal

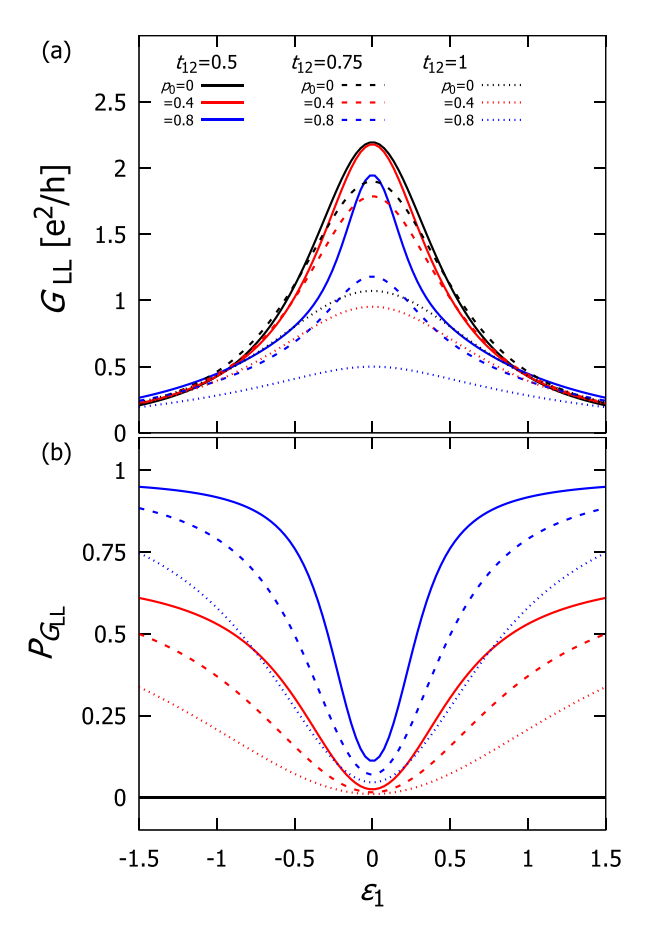


FIG. 9. (a) The local conductance G_{LL} and (b) its polarization $P_{G_{LL}}$ as a function of the energy level ε_1 obtained for various t_{12} and p_0 , as indicated. Results are obtained for $\varepsilon_2 = 0$, $\Gamma_S = 2$, $\Gamma_L = \Gamma_R = 0.5$, and $k_B T = 0.05$.

conductance [Fig. 10(b)] reveals divergence points which indicate a changeover of the dominant transport channel. Such points are sensitive to the polarization and occur only for sufficiently strong interdot coupling $t_{12} > 0.5$. The differential conductance, together with its polarized version, provides valuable information about the leading transport channel of our multiterminal superconducting junction, which is particularly useful in the presence of external fields.

C. Thermopower of the polarized system

Polarization of the external leads has an effect on the Seebeck coefficients. Let us recall that in N-QD-N junctions the thermopower is determined by the slope of the quantum dot spectral function $\partial A_{\sigma}(\omega)/\partial \omega$ at the Fermi level ($\omega=0$) [61]. In the weak interdot coupling limit of our setup and in the absence of polarization, the spectrum of QD₁ is represented by a Lorentzian peak centered at ε_1 (Fig. 3); therefore, the local thermopower [Fig. 11(a)] has the usual sawtooth shape. Polarization induces splitting of the quasiparticle state at $\omega \sim \varepsilon_1$ (Fig. 8), which partly flattens the net thermopower.

Qualitative changes, however, can be noticed in the spinresolved Seebeck coefficient defined in Eq. (41). In the presence of polarization, for $\varepsilon_1 < 0$ and weak interdot coupling we obtain $\partial A_{\uparrow}/\partial \omega(\varepsilon_F) > \partial A_{\downarrow}/\partial \omega(\varepsilon_F)$; therefore, the

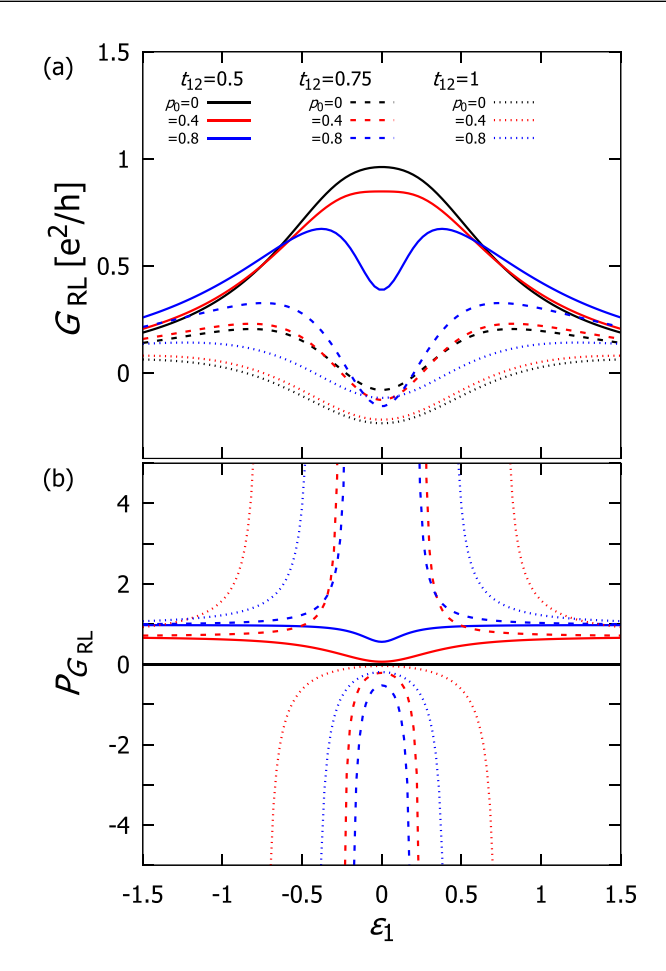


FIG. 10. Variation of (a) the nonlocal conductance G_{RL} and (b) its polarization $P_{G_{RL}}$ with respect to the energy level ε_1 obtained for several values of t_{12} and p_0 , using the model parameters $\varepsilon_2 = 0$, $\Gamma_S = 2$, $\Gamma_L = \Gamma_R = 0.5$, and $k_B T = 0.05$.

spin-resolved thermopower is positive. With increasing t_{12} , the polarization amplifies the splitting of $A_{\uparrow}(\omega)$ sector and suppresses the spectral weight of $A_{\downarrow}(\omega)$. In effect, the thermopower $S_{LL}(S)$ [Fig. 11(b)] reverses sign due to the combined influence of the electron pairing and the polarization imposed on the central quantum dot.

The spin-resolved Seebeck coefficient is thus a sensitive probe of the superconducting proximity effect (transmitted to QD_1 via interdot coupling) competing with polarization effects.

V. SUMMARY

We studied the quasiparticle spectrum and transport properties of a double quantum dot embedded in T-shaped geometry between two conducting (or ferromagnetic) leads and strongly hybridized with superconducting electrode. In this configuration the proximity effect induces the bound states on the quantum dot adjacent to the superconductor (QD_2) , which then is partly or entirely transmitted to the other dot (QD_1) . In the weak interdot coupling regime this process leads to the appearance of Fano-like structures in the spectrum of QD_1 , whereas the tightly bound quantum dots develop the molecular structure of their Andreev states. These phenomena

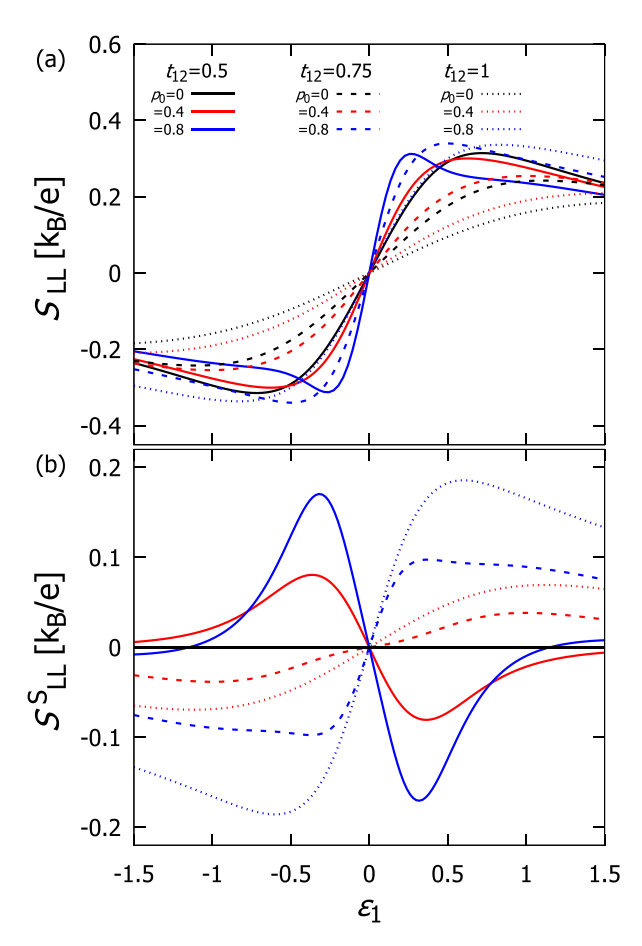


FIG. 11. (a) The local thermopower S_{LL} and (b) the spin-resolved thermopower S_{LL}^S as a function of the QD₁ energy level obtained for several values of t_{12} and p_0 , assuming the model parameters $\varepsilon_2 = 0$, $\Gamma_S = 2$, $\Gamma_L = \Gamma_R = 0.5$, and $k_B T = 0.05$.

qualitatively affect the charge transport and thermoelectric properties of the setup.

We thoroughly analyzed the influence of the interdot coupling t_{12} on the transport coefficients which could be experimentally accessible. Specifically, we examined the variation of the local and nonlocal conductances and thermoelectric coefficients with increasing t_{12} . We found that in the weak coupling limit the ballistic transport becomes reduced (by destructive quantum interference), whereas the direct and crossed Andreev scatterings are gradually amplified (by the superconducting proximity effect indirectly transmitted onto QD₁). This tendency is clearly reflected in the local electric conductance (Figs. 5 and 6) and is even more pronounced in the nonlocal conductance, revealing a competition between the ballistic electron tunneling and the crossed Andreev reflection (29). The latter undergoes suppression with increasing t_{12} and eventually reverses sign when the crossed Andreev reflections become the dominant transport channel.

We also examined how the interdot coupling affects the local and nonlocal thermopower. For the weak interdot coupling we found that the local Seebeck coefficient acquires the usual sawtooth shape as a function of the quantum dot energy level (caused by the changeover from the particle- to holedominated single particle charge transfer). In contrast, for

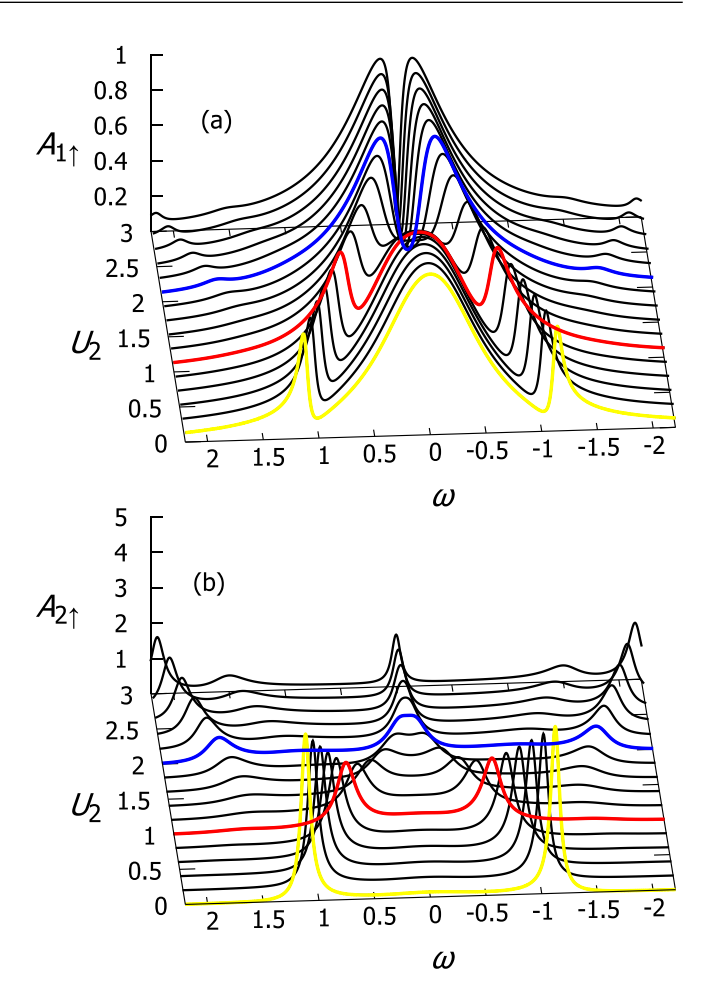


FIG. 12. The normalized spectral function $A_{i\uparrow}(\omega)$ of the (a) first and (b) second quantum dots as a function of the Coulomb repulsion U_2 . Other parameters are $\varepsilon_1=0$, $\varepsilon_2=-U_2/2$, $\Gamma_S=2$, $\Gamma_L=\Gamma_R=0.5$, $t_BT=0$, $t_BT=0$, and $t_{12}=0.4$.

large coupling t_{12} , we obtained qualitatively different behavior which manifests the superconductivity-proximity-dominated regime. In particular, it reveals the divergence point.

In the setup with ferromagnetic electrodes the ballistic transport channel is dependent on the individual spin components. For this reason we investigated in detail the spin-resolved conductance and the Seebeck coefficients in both their local and nonlocal versions. The resulting transport coefficient reveals a subtle interplay between the spin-resolved ballistic transfer and the Andreev scatterings, which equally engage both spin components.

In summary, we showed that charge transport measurements are able to probe the efficiency of the superconducting proximity effect imposed on the double quantum dot in three-terminal hybrid structures. Transport properties can clearly distinguish the molecular bound states (when the interdot coupling is strong) from different situations where the ingap states are formed merely in one of the dots while the second one is affected by interferometric (Fano-type) effects. These phenomena could also be encountered in other hybrid architectures, for instance, using two quantum dots attached to Majorana modes [46]. Furthermore, similar effects might show up when one inspects the parity of the Andreev molecule

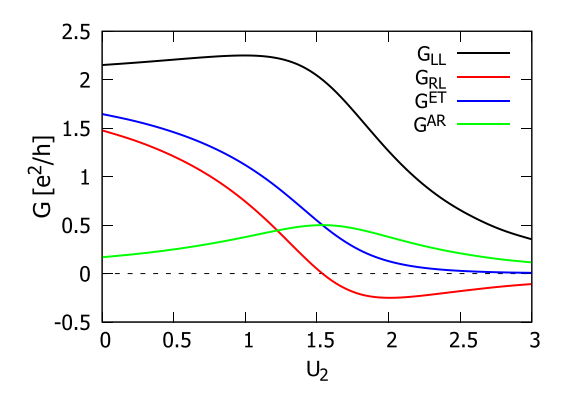


FIG. 13. The zero-bias conductance (local G_{LL} , black line; non-local G_{RL} , red line; electron tunneling $G^{\rm ET}$, blue line; and Andreev reflection $G^{\rm AR} = G^{\rm DAR} = G^{\rm CAR}$, green line) as a function of the Coulomb repulsion U_2/Γ_N . Results are obtained for $\varepsilon_1 = 0$, $\varepsilon_2 = -U_2/2$, $\Gamma_S = 2$, $\Gamma_L = \Gamma_R = 0.5$, T = 0, $P_0 = 0$, and $P_1 = 0.4$.

of two quantum dots interconnected via a superconducting reservoir [62,63]. The latter scenario is now considered a possible means for the realization of the minimal Kitaev model hosting poor man's Majorana quasiparticles [64].

ACKNOWLEDGMENT

This research project was supported by the National Science Centre (Poland) through Grant No. 2022/04/Y/ST3/00061.

DATA AVAILABILITY

The data that support the findings of this article are openly available [65].

APPENDIX A: CORRELATION EFFECTS

Under specific conditions, the spectra of the quantum dots can additionally be influenced by Coulomb repulsion between opposite spin electrons $U_i d_{i\uparrow}^\dagger d_{i\uparrow} d_{i\downarrow}^\dagger d_{i\downarrow}$. We shall discuss the major effects arising from such interactions, inspecting their role at each dot (i=1,2) separately.

The repulsive potential U_2 of the quantum dot directly attached to the superconductor can be expected to compete with the proximity effect. Signatures of this competition are evident already within the mean field approximation (valid for $U_2 \ll \Gamma_S$), leading to renormalization of the on-dot pairing potential $\frac{\Gamma_s}{2} \to \frac{\Gamma_s}{2} - U_2 \langle d_{2\downarrow} d_{2\uparrow} \rangle$. With the use of more sophisticated methods to treat the Hamiltonian of QD₂ [66], substantial changes in the Andreev bound states have been predicted. In particular, by varying U_2/Γ_s the ratio or the energy level ε_2 the ground state of QD₂ eventually undergoes the quantum phase transition between the BCS-type (spinless) and singly occupied (spinful) configurations [6]. For the particle-hole symmetric case ($\varepsilon_2 = -U_2/2$), this quantum phase transition occurs at $U_2 = \Gamma_S$. In the strong interaction limit, $U_2 > \Gamma_S$, the on-dot pairing $\langle d_{2\downarrow} d_{2\uparrow} \rangle$ is strongly (or completely) suppressed. The influence of such effects on the local and nonlocal conductances of the three-terminal junction comprising the single quantum dot was recently addressed in Ref. [20]. Here, in the setup with the double quantum dot, the Coulomb potential could predominantly affect the transport channels contributed by the Andreev scattering.

Figure 12 shows the quasiparticle spectrum of spin- \uparrow electrons of both quantum dots obtained for the particle-hole symmetric case, $\varepsilon_2 = -U_2/2$ (neglecting the Coulomb potential $U_1 = 0$). Numerical results for the Green's function matrix were obtained with the self-consistent second-order perturbation theory [18,19,67]. Inspecting $A_{2\uparrow}(\omega)$, we can clearly see the singlet-doublet changeover that occurs near $U_2 \approx \Gamma_S$ (strictly speaking, it is no longer sharp due to the interdot coupling). In the spectrum of QD₂ adjacent to the superconducting lead [Fig. 12(b)], we observe two Andreev states which merge at $U_2 \rightarrow \Gamma_S$. In contrast, in the strong

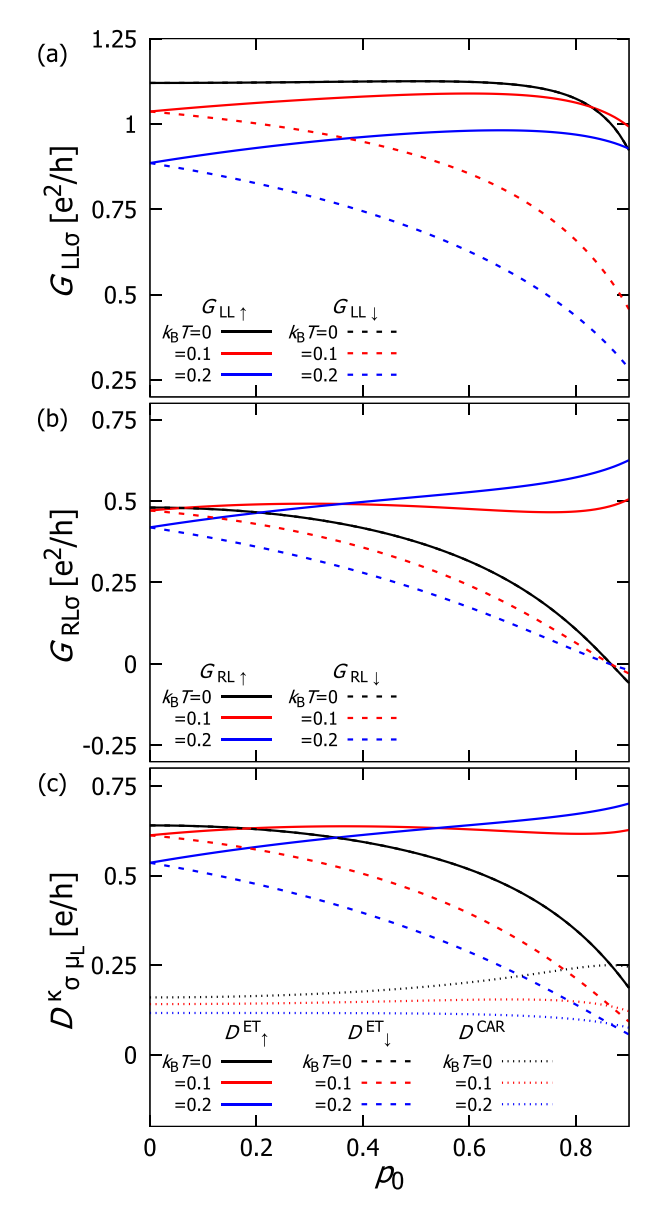


FIG. 14. Variation of the (a) local, G_{LL} , and (b) nonlocal, G_{RL} , spin-dependent conductivities and (c) the transport coefficients $D_{\sigma\mu_L}^{\kappa}$ versus the polarization p_0 , obtained for several temperatures using the model parameters $\varepsilon_1 = \varepsilon_2 = 0$, $\Gamma_S = 2$, $\Gamma_L = \Gamma_R = 0.5$, and $t_{12} = 0.5$.

interaction limit, the Abrikosov-Suhl state develops at the Fermi level, $\omega=0$, originating from the antiferromagnetic exchange interactions of QD₂ with mobile electrons from external metallic leads [13]. In addition to this Kondo feature, there are also other quasiparticles with finite energies that represent molecular Andreev states [6]. On the other hand, the spectrum of QD₁ [Fig. 12(a)] reveals completely different line shapes. At energies corresponding to the Andreev peaks (in the weak interaction limit, $U_2 < \Gamma_s$) we observe resonantlike dip structures, and (in the strong interaction regime, $U_2 > \Gamma_s$) another depleted region is observed around the Kondo state.

The influence of the Coulomb potential U_2 on the local and nonlocal transport properties of our system is presented in Fig. 13. We notice that upon traversing the singlet-doublet transition, the ballistic electron transfer (blue line in Fig. 13) is gradually suppressed. In contrast, the Andreev conductance achieves optimal values around this crossover region (where the molecular quasiparticle energies cross each other). A further consequence of this behavior is observed in the nonlocal conductance (displayed by the red line), which changes sign to negative values near the singlet-doublet crossover.

Concerning the Coulomb interactions U_1 , its influence is qualitatively different from that discussed above. Repulsive interactions at QD₁ mainly affect the ballistic transport channel, being less efficient for Andreev scattering. The resulting effect is hence reminiscent of the Coulomb blockade. Its signatures could be observed by enhancing the differential conductance at $\omega = \varepsilon_1$ and $\varepsilon_1 + U_1$ due to the charging effects. Furthermore, at low temperatures, the Abrikosov-Suhl

peak can be induced by the effective exchange interactions between the mobile electrons of the metallic leads and the localized electron on QD₁. Such Kondo physics would lead to the enhancement of the zero-bias conductance of the single electron (ballistic) channel. Further indirect effects on the proximity-induced electron pairing would be less meaningful unless the interdot coupling is strong. Major aspects related to the latter mechanism were studied by Calle *et al.* [46]; therefore, we skip their discussion.

APPENDIX B: POLARIZED TRANSPORT COEFFICIENTS

In this appendix we briefly consider the influence of temperature on the transport coefficients, originating from the Fermi-Dirac distribution function entering the expressions for charge current. Figure 14 shows the local, G_{LL} , and nonlocal, G_{RL} , spin-dependent conductivities with respect to the polarization of electrodes p_0 obtained in the electron-hole symmetric case, $\varepsilon_1 = 0 = \varepsilon_2$, and for several temperatures. For T=0 (black lines), the zero-bias conductivity is proportional to the transmittance at $\omega = 0$; therefore, $G_{LL(RL)\uparrow} =$ $G_{LL(RL)\downarrow}$. By increasing the polarization, we observe suppression of $T_{\sigma}^{\text{ET}}(0)$ and a slight enhancement of $T_{\sigma}^{\text{DAR(CAR)}}(0)$. Consequently, the local conductance $G_{LL\sigma}$ weakly depends on p_0 , whereas the nonlocal conductance $G_{RL\sigma}$ reveals a gradual reduction. At finite temperatures, T > 0, we obtain the spin-dependent conductance $G_{LL(RL)\uparrow} \neq G_{LL(RL)\downarrow}$ for arbitrary values of $p_0 \neq 0$. In this case, nonvanishing spin polarization of the local and nonlocal conductance can be observed.

- [14] J.-D. Pillet, P. Joyez, R. Žitko, and M. F. Goffman, Tunneling spectroscopy of a single quantum dot coupled to a superconductor: From Kondo ridge to Andreev bound states, Phys. Rev. B 88, 045101 (2013).
- [15] B.-K. Kim, Y.-H. Ahn, J.-J. Kim, M.-S. Choi, M.-H. Bae, K. Kang, J. S. Lim, R. López, and N. Kim, Transport measurement of Andreev bound states in a Kondo-correlated quantum dot, Phys. Rev. Lett. 110, 076803 (2013).
- [16] J. He, D. Pan, G. Yang, M. Liu, J. Ying, Z. Lyu, J. Fan, X. Jing, G. Liu, B. Lu, D. E. Liu, J. Zhao, L. Lu, and F. Qu, Nonequilibrium interplay between Andreev bound states and Kondo effect, Phys. Rev. B 102, 075121 (2020).

^[1] P. Krantz, M. Kjaergaard, F. Yan, T. P. Orlando, S. Gustavsson, and W. D. Oliver, A quantum engineer's guide to superconducting qubits, Appl. Phys. Rev. 6, 021318 (2019).

^[2] M. Benito and G. Burkard, Hybrid superconductor-semiconductor systems for quantum technology, Appl. Phys. Lett. 116, 190502 (2020).

^[3] G. P. Mazur, N. van Loo, D. van Driel, J.-Y. Wang, G. Badawy, S. Gazibegovic, E. P. A. M. Bakkers, and L. P. Kouwenhoven, Gate-tunable Josephson diode, Phys. Rev. Appl. 22, 054034 (2024).

^[4] X. Liu, X. Li, D.-L. Deng, X.-J. Liu, and S. Das Sarma, Majorana spintronics, Phys. Rev. B 94, 014511 (2016).

^[5] R. Aguado, A perspective on semiconductor-based superconducting qubits, Appl. Phys. Lett. 117, 240501 (2020).

^[6] J. Bauer, A. Oguri, and A. C. Hewson, Spectral properties of locally correlated electrons in a Bardeen-Cooper-Schrieffer superconductor, J. Phys.: Condens. Matter 19, 486211 (2007).

^[7] A. Martín-Rodero and A. L. Yeyati, Josephson and Andreev transport through quantum dots, Adv. Phys. 60, 899 (2011).

^[8] A. Eichler, M. Weiss, S. Oberholzer, C. Schönenberger, A. Levy Yeyati, J. C. Cuevas, and A. Martín-Rodero, Even-odd effect in Andreev transport through a carbon nanotube quantum dot, Phys. Rev. Lett. 99, 126602 (2007).

^[9] R. S. Deacon, Y. Tanaka, A. Oiwa, R. Sakano, K. Yoshida, K. Shibata, K. Hirakawa, and S. Tarucha, Tunneling spectroscopy

of Andreev energy levels in a quantum dot coupled to a superconductor, Phys. Rev. Lett. **104**, 076805 (2010).

^[10] J.-D. Pillet, C. H. L. Quay, P. Morfin, C. Bena, A. Levy Yeyati, and P. Joyez, Andreev bound states in supercurrent-carrying carbon nanotubes revealed, Nat. Phys. 6, 965 (2010).

^[11] T. Dirks, T. L. Hughes, S. Lal, B. Uchoa, Y.-F. Chen, C. Chialvo, P. M. Goldbart, and N. Mason, Transport through Andreev bound states in a graphene quantum dot, Nat. Phys. 7, 386 (2011).

^[12] R. Žitko, J. S. Lim, R. López, and R. Aguado, Shiba states and zero-bias anomalies in the hybrid normal-superconductor Anderson model, Phys. Rev. B 91, 045441 (2015).

^[13] T. Domański, I. Weymann, M. Barańska, and G. Górski, Constructive influence of the induced electron pairing on the Kondo state, Sci. Rep. 6, 23336 (2016).

- [17] Y. Yamada, Y.i Tanaka, and N. Kawakami, Enhanced Andreev tunneling via the Kondo resonance in a quantum dot at finite bias, J. Phys. Soc. Jpn. **79**, 043705 (2010).
- [18] Y. Yamada, Y. Tanaka, and N. Kawakami, Interplay of Kondo and superconducting correlations in the nonequilibrium Andreev transport through a quantum dot, Phys. Rev. B 84, 075484 (2011).
- [19] G. Górski, J. Barański, I. Weymann, and T. Domański, Interplay between correlations and Majorana mode in proximitized quantum dot, Sci. Rep. 8, 15717 (2018).
- [20] M. Hashimoto, Y. Yamada, Y. Tanaka, Y. Teratani, T. Kemi, N. Kawakami, and A. Oguri, Nonlocal andreev transport through a quantum dot in a magnetic field: Interplay between Kondo, Zeeman, and Cooper-pair correlations, Phys. Rev. B 109, 035404 (2024).
- [21] S.-Y. Hwang, R. López, and D. Sánchez, Large thermoelectric power and figure of merit in a ferromagnetic–quantum dot– superconducting device, Phys. Rev. B 94, 054506 (2016).
- [22] S.-Y. Hwang, D. Sánchez, and R. López, A hybrid superconducting quantum dot acting as an efficient charge and spin Seebeck diode, New J. Phys. 18, 093024 (2016).
- [23] S. Verma and A. Singh, Seebeck power generation and peltier cooling in a normal metal-quantum dot-superconductor nanodevice, J. Low Temp. Phys. 214, 344 (2024).
- [24] G. Michałek, B. R. Bułka, T. Domański, and K. I. Wysokiński, Interplay between direct and crossed Andreev reflections in hybrid nanostructures, Phys. Rev. B 88, 155425 (2013).
- [25] I. Weymann and P. Trocha, Superconducting proximity effect and zero-bias anomaly in transport through quantum dots weakly attached to ferromagnetic leads, Phys. Rev. B 89, 115305 (2014).
- [26] K. P. Wójcik and I. Weymann, Proximity effect on spindependent conductance and thermopower of correlated quantum dots, Phys. Rev. B 89, 165303 (2014).
- [27] E. C. Siqueira, P. A. Orellana, R. C. Cestari, M. S. Figueira, and G. G. Cabrera, Fano effect and Andreev bound states in a hybrid superconductor–ferromagnetic nanostructure, Phys. Lett. A 379, 2524 (2015).
- [28] G. Michałek, M. Urbaniak, B. R. Bułka, T. Domański, and K. I. Wysokiński, Local and nonlocal thermopower in three-terminal nanostructures, Phys. Rev. B 93, 235440 (2016).
- [29] J. Gramich, A. Baumgartner, and C. Schönenberger, Andreev bound states probed in three-terminal quantum dots, Phys. Rev. B 96, 195418 (2017).
- [30] F. Pawlicki and I. Weymann, Andreev transport through single-molecule magnets, Phys. Rev. B 98, 085411 (2018).
- [31] F. Mazza, R. Bosisio, G. Benenti, V. Giovannetti, R. Fazio, and F. Taddei, Thermoelectric efficiency of three-terminal quantum thermal machines, New J. Phys. 16, 085001 (2014).
- [32] B. M. Andersen, K. Flensberg, V. Koerting, and J. Paaske, Nonequilibrium transport through a spinful quantum dot with superconducting leads, Phys. Rev. Lett. 107, 256802 (2011).
- [33] A. P. Higginbotham, S. M. Albrecht, G. Kiršanskas, W. Chang, F. Kuemmeth, P. Krogstrup, T. S. Jespersen, J. Nygård, K. Flensberg, and C. M. Marcus, Parity lifetime of bound states in a proximitized semiconductor nanowire, Nat. Phys. 11, 1017 (2015).
- [34] R. Sánchez and M. Büttiker, Optimal energy quanta to current conversion, Phys. Rev. B **83**, 085428 (2011).

- [35] H. Thierschmann, R. Sánchez, B. Sothmann, F. Arnold, C. Heyn, W. Hansen, H. Buhmann, and L. W. Molenkamp, Three-terminal energy harvester with coupled quantum dots, Nat. Nanotechnol. 10, 854 (2015).
- [36] B. Szukiewicz and K. I. Wysokiński, Quantum dot as spin current generator and energy harvester, Eur. Phys. J. B 88, 112 (2015).
- [37] B. Sothmann, R. Sánchez, and A. N. Jordan, Thermoelectric energy harvesting with quantum dots, Nanotechnology 26, 032001 (2015).
- [38] A. Oguri and Y. Tanaka, Transport through a single Anderson impurity coupled to one normal and two superconducting leads, J. Phys.: Conf. Ser. 391, 012146 (2012).
- [39] A. Oguri, Y. Tanaka, and J. Bauer, Interplay between Kondo and Andreev-Josephson effects in a quantum dot coupled to one normal and two superconducting leads, Phys. Rev. B 87, 075432 (2013).
- [40] G. Kiršanskas, M. Goldstein, K. Flensberg, L. I. Glazman, and J. Paaske, Yu-Shiba-Rusinov states in phase-biased superconductor-quantum dot-superconductor junctions, Phys. Rev. B 92, 235422 (2015).
- [41] T. Domański, M. Žonda, V. Pokorný, G. Górski, V. Janiš, and T. Novotný, Josephson-phase-controlled interplay between correlation effects and electron pairing in a three-terminal nanostructure, Phys. Rev. B 95, 045104 (2017).
- [42] E. C. Siqueira and G. G. Cabrera, Magnetoresistance and transistor-like behavior of a double quantum-dot via crossed andreev reflections, J. Appl. Phys. 111, 113905 (2012).
- [43] A. M. Calle, M. Pacheco, and P. A. Orellana, Fano effect and Andreev bound states in T-shape double quantum dots, Phys. Lett. A 377, 1474 (2013).
- [44] A. M. Calle, M. Pacheco, G. B. Martins, V. M. Apel, G. A. Lara, and P. A. Orellana, Fano–Andreev effect in a T-shape double quantum dot in the Kondo regime, J. Phys.: Condens. Matter 29, 135301 (2017).
- [45] K. P. Wójcik and I. Weymann, Interplay of the Kondo effect with the induced pairing in electronic and caloric properties of T-shaped double quantum dots, Phys. Rev. B 97, 235449 (2018).
- [46] A. M. Calle, Mónica Pacheco, P. A. Orellana, and J. A. Otálora, Fano-Andreev and Fano-Majorana correspondence in quantum dot hybrid structures, Ann. Phys. (Berlin) 532, 1900409 (2020).
- [47] A. González Inostroza, I. A. M. Calle, M. Pacheco, E. C. Siqueira, and P. A. Orellana, Fano-Andreev effect in a T-shaped double quantum dot in the Coulomb blockade regime, Eur. Phys. J. Plus 139, 790 (2024).
- [48] L. M. Rütten, H. Schmid, E. Liebhaber, G. Franceschi, A. Yazdani, G. Reecht, K. Rossnagel, F. von Oppen, and K. J. Franke, Wave function engineering on superconducting substrates: Chiral Yu-Shiba-Rusinov molecules, ACS Nano 18, 30798 (2024).
- [49] C. Li, V. Pokorný, M. Žonda, J.-C. Liu, P. Zhou, O. Chahib, T. Glatzel, R. Häner, S. Decurtins, S.-X. Liu, R. Pawlak, and E. Meyer, Individual assembly of radical molecules on superconductors: Demonstrating quantum spin behavior and bistable charge rearrangement, ACS Nano 19, 3403 (2025).
- [50] C. Ortega-Taberner, A.-P. Jauho, and J. Paaske, Anomalous Josephson current through a driven double quantum dot, Phys. Rev. B 107, 115165 (2023).

- [51] P. Zhang, H. Wu, J. Chen, S. A. Khan, P. Krogstrup, D. Pekker, and S. M. Frolov, Signatures of Andreev blockade in a double quantum dot coupled to a superconductor, Phys. Rev. Lett. 128, 046801 (2022).
- [52] Z.-J. Li, Y.-H. Jin, Y.-H. Nie, and J.-Q. Liang, Electron transport through double quantum dots with spin-polarization dependent interdot coupling, J. Phys.: Condens. Matter 20, 085214 (2008).
- [53] Q. Wang, H.-Q. Xie, H.-J. Jiao, Z.-J. Li, and Y.-H. Nie, Spin-dependent thermoelectric transport through double quantum dots, Chin. Phys. B 21, 117310 (2012).
- [54] H. Yao, C. Zhang, P.-B. Niu, Z.-J. Li, and Y.-H. Nie, Enhancement of charge and spin Seebeck effect in triple quantum dots coupling to ferromagnetic and superconducting electrodes, Phys. Lett. A 382, 3220 (2018).
- [55] H. Haug and A.-P. Jauho, *Quantum Kinetics in Transport and Optics of Semiconductors*, Springer Series in Solid-State Sciences (Springer, Berlin, 2008), Vol. 123.
- [56] R. Świrkowicz, M. Wierzbicki, and J. Barnaś, Thermoelectric effects in transport through quantum dots attached to ferromagnetic leads with noncollinear magnetic moments, Phys. Rev. B 80, 195409 (2009).
- [57] I. Weymann and J. Barnaś, Spin thermoelectric effects in Kondo quantum dots coupled to ferromagnetic leads, Phys. Rev. B 88, 085313 (2013).
- [58] G. Michałek, T. Domański, B. R. Bułka, and K. I. Wysokiński, Novel non-local effects in three-terminal hybrid devices with quantum dot, Sci. Rep. 5, 14572 (2015).
- [59] A. Manaparambil and I. Weymann, Nonequilibrium Seebeck effect and thermoelectric efficiency of Kondo-correlated molecular junctions, Phys. Rev. B 107, 085404 (2023).

- [60] S. Valentini, R. Fazio, V. Giovannetti, and F. Taddei, Thermopower of three-terminal topological superconducting systems, Phys. Rev. B 91, 045430 (2015).
- [61] T. A. Costi and V. Zlatić, Thermoelectric transport through strongly correlated quantum dots, Phys. Rev. B 81, 235127 (2010).
- [62] M. Geier, R. S. Souto, J. Schulenborg, S. Asaad, M. Leijnse, and K. Flensberg, Fermion-parity qubit in a proximitized double quantum dot, Phys. Rev. Res. 6, 023281 (2024).
- [63] D. van Driel, B. Roovers, F. Zatelli, A. Bordin, G. Wang, N. van Loo, J. C. Wolff, G. P. Mazur, S. Gazibegovic, G. Badawy, E. P. A. M. Bakkers, L. P. Kouwenhoven, and T. Dvir, Charge sensing the parity of an Andreev molecule, PRX Quantum 5, 020301 (2024).
- [64] T. Dvir, G. Wang, N. van Loo, C. X. Liu, G. P. Mazur, A. Bordin, S. L. D. Ten Haaf, J. Y. Wang, D. van Driel, F. Zatelli, X. Li, F. K. Malinowski, S. Gazibegovic, G. Badawy, E. P. A. M. Bakkers, M. Wimmer, and L. P. Kouwenhoven, Realization of a minimal Kitaev chain in coupled quantum dots, Nature (London) 614, 445 (2023).
- [65] G. Górski, T. Domański, and K. Kucab, Numerical data for "Properties of multiterminal superconducting nanostructure with double quantum dot" [Data set], Zenodo (2025), https://doi.org/10.5281/zenodo.15223807.
- [66] V. Pokorný and M. Žonda, Effective low-energy models for superconducting impurity systems, Phys. Rev. B 107, 155111 (2023).
- [67] E. Vecino, A. Martín-Rodero, and A. L. Yeyati, Josephson current through a correlated quantum level: Andreev states and π junction behavior, Phys. Rev. B **68**, 035105 (2003).